

Article

In Silico Pesticide Discovery for New Anti-Tobacco Mosaic Virus Agents: Reactivity, Molecular Docking, and Molecular Dynamics Simulations

Hala A. Abdulhassan ¹, Basil A. Saleh ^{2,*}, Dalal Harkati ³, Hadjer Khelifaoui ³, Natalie L. Hewitt ⁴
and Gamal A. El-Hiti ^{5,*}

- ¹ Department of Plant Protection, College of Agriculture, University of Basrah, Basrah 61004, Iraq; halaa.abduljabbar@uobasrah.edu.iq
- ² Department of Chemistry, College of Science, University of Basrah, Basrah 61004, Iraq
- ³ Group of Computational and Pharmaceutical Chemistry, LMCE Laboratory, Faculty of Exact and Natural Sciences, Department of Matter Sciences, University of Biskra, Biskra 07000, Algeria; d.harkati@univ-biskra.dz (D.H.); hadjer.khelifaoui@univ-biskra.dz (H.K.)
- ⁴ Norgine Limited, New Road, Tir-Y-Berth, Hengoed CF82 8SJ, UK; nhewitt@norgine.com
- ⁵ Department of Optometry, College of Applied Medical Sciences, King Saud University, Riyadh 11433, Saudi Arabia
- * Correspondence: basil.saleh@uobasrah.edu.iq (B.A.S.); gelhiti@ksu.edu.sa (G.A.E.-H.); Tel.: +96-61-1469-3778 (G.A.E.-H.); Fax: +96-61-1469-3536 (G.A.E.-H.)

Abstract: Considerable data are available regarding the molecular genetics of the *tobacco mosaic virus*. The disease caused by the *tobacco mosaic virus* is still out of control due to the lack of an efficient functional antagonist chemical molecule. Extensive research was carried out to try to find effective new anti-tobacco mosaic virus agents, however no study could find an effective agent which could completely inhibit the disease caused by the virus. In recent years, molecular docking, combined with molecular dynamics, which is considered to be one of the most important methods of drug discovery and design, were used to evaluate the type of binding between the ligand and its protein enzyme. The aim of the current work was to assess the *in silico* anti-tobacco mosaic virus activity for a selection of 41 new and 2 reference standard compounds. These compounds were chosen to examine their reactivity and binding efficiency with the tobacco mosaic virus coat protein (PDB ID: 2OM3). A comparison was made between the activity of the selected compounds and that for ningnanmycin and ribavirin, which are common inhibitors of plant viruses. The simulation results obtained from the molecular docking and molecular dynamics showed that two compounds of the antifine analogues could bind with the tobacco mosaic virus coat protein receptor better than ningnanmycin and ribavirin.

Keywords: anti-tobacco mosaic virus; molecular docking; molecular dynamics; ningnanmycin; ribavirin; antifine analogues



Citation: Abdulhassan, H.A.; Saleh, B.A.; Harkati, D.; Khelifaoui, H.; Hewitt, N.L.; El-Hiti, G.A. *In Silico* Pesticide Discovery for New Anti-Tobacco Mosaic Virus Agents: Reactivity, Molecular Docking, and Molecular Dynamics Simulations. *Appl. Sci.* **2022**, *12*, 2818. <https://doi.org/10.3390/app12062818>

Academic Editor: Kirill Glavatskiy

Received: 21 January 2022

Accepted: 8 March 2022

Published: 9 March 2022

Publisher's Note: MDPI stays neutral with regard to jurisdictional claims in published maps and institutional affiliations.



Copyright: © 2022 by the authors. Licensee MDPI, Basel, Switzerland. This article is an open access article distributed under the terms and conditions of the Creative Commons Attribution (CC BY) license (<https://creativecommons.org/licenses/by/4.0/>).

1. Introduction

Plant diseases caused by viruses are causing severe economic damage to the agricultural industry and seriously affect its development [1–4]. The tobacco mosaic virus (TMV; *Tobamovirus* genus) is one of the most common destructive phytopathogens [5,6]. It infects more than 400 crops that have economic importance, including tobacco, vegetables, and ornamental flowers [7]. The TMV is known as plants cancer and causes fruit and leaf deformation, plant dwarfing, and a reduction in seed germination rates [8,9]. The complete protection of plants against TMV infection presents a difficult challenge, since no efficient antiviral reagent has not yet been found. Ribavirin and ningnanmycin are widely used as antiviral reagents against TMV infection [10,11]. Ningnanmycin and ribavirin have a moderate control effect (50–60% at 500 µg/mL) against the TMV [12,13]. Clearly, the curatives rate of these antiviral reagents

is unsatisfactory, and therefore considerable attention was paid towards the screening, design, synthesis, and use of new compounds that have potential biological activity [14]. Some progress has been made with the design and use of effective antiviral agents to protect plants against specific diseases. For example, zinc oxide nanoparticles were found to be effective to protect tomato plants against the *tomato mosaic virus* [15]. In addition, salicylic acid and melatonin act as antiviral agents to protect eggplant against *alfalfa mosaic virus* without posing a danger or being hazardous to the environment [16].

Many attempts were made to design and synthesize new and efficient anti-TMV agents [17–22]. New anti-TMV agents should be designed to have low toxicity, rapid degradation in the environment, and a unique mode of action. Many natural products-based agrochemicals were assessed for their use as anti-TMV agents. Research has continued to find potential alternative pesticides that do not pose a hazard to the environment [23–27]. Few *in silico* studies related to the TMV have been conducted [28–30]. For example, a series of ureas and thioureas containing heterocyclic compounds (e.g., pyrimidine and piperazine moieties) were studied to investigate their TMV inhibitors. The molecular docking and molecular dynamics simulations were used to understand the interaction between the TMV coat protein and the synthesized compounds. A good agreement was found between the *in silico* analysis and the experimental results [28]. However, there is an urgent need to find a new anti-TMV agent that is capable of preventing such a disease.

The current study aimed to assess the *in silico* anti-TMV activity of 43 compounds of antifine analogue, including ningnanmycin (1) and ribavirin (2). The selected compounds were reported to have varied anti-TMV activity [9,14,24–27,31]. The chemical structures of the compounds are shown in Table 1. The reactivity of these compounds and their binding with the tobacco mosaic virus coat protein (TMV-CP) were simulated and compared with standard anti-TMV agents (e.g., ningnanmycin 1 and ribavirin 2) using the Gaussian 09 software with the B3LYP/6-31G basis set [32] and the molecular operation environment (MOE) software [33].

Table 1. The inhibition rate (%) of the antifine analogues 1–43 against TMV and their smiles.

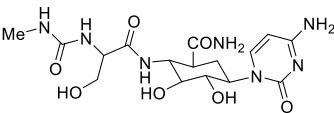
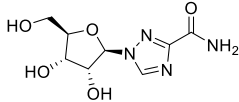
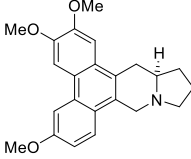
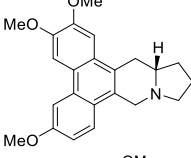
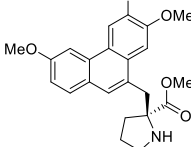
Compd	Structure	Smiles	Inhibition Rate (%)	Ref
1		<chem>O=C(N[C@H]1[C@H](O)[C@@H](O)[C@H](N2C(=O)N=C(N)C=C2)O[C@@H]1C(=O)N)[C@@H](NC(=O)CNC)CO</chem>	69.3	[14]
2		<chem>O=C(N)c1nn([C@H]2[C@H](O)[C@H](O)[C@@H](CO)O2)cn1</chem>	41.3	[14]
3		<chem>O(C)c1c(OC)cc2c(c3c(c4c2C[C@H]2[N@@](C4)CC2)ccc(OC)c3)c1</chem>	65.8	[14]
4		<chem>O(C)c1c(OC)cc2c(c3c(c4c2C[C@H]2[N@@](C4)CCC2)ccc(OC)c3)c1</chem>	60.2	[14]
5		<chem>O=C(OC)[C@]1(Cc2c3c(c4c(c2)ccc(OC)c4)cc(OC)c(OC)c3)NCCC1</chem>	62.5	[14]

Table 1. Cont.

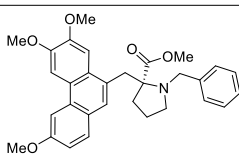
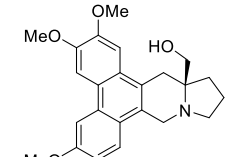
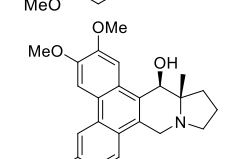
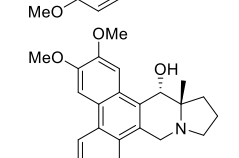
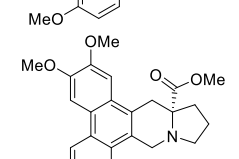
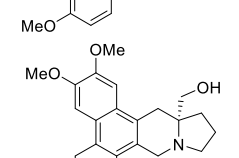
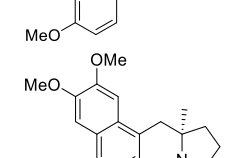
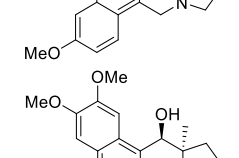
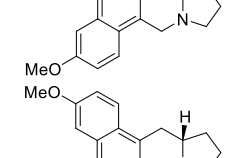
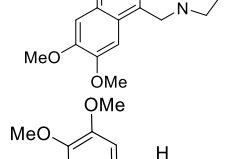
Compd	Structure	Smiles	Inhibition Rate (%)	Ref
6		<chem>O=C(OC)[C@]1(Cc2c3c(c4c(c2)ccc(OC)c4)cc(OC)c(OC)c3)[N@](Cc2ccccc2)CCC1</chem>	60.0	[14]
7		<chem>O(C)c1c(OC)cc2c(c3c(c4c2C[C@@]2(CO)[N@@](C4)CC(C2)ccc(OC)c3)c1</chem>	58.9	[14]
8		<chem>O(C)c1c(OC)cc2c(c3c(c4c2[C@@H](O)[C@@]2(C)[N@@](C4)CCC2)ccc(OC)c3)c1</chem>	61.4	[14]
9		<chem>O(C)c1c(OC)cc2c(c3c(c4c2[C@H](O)[C@@]2(C)[N@@](C4)CCC2)ccc(OC)c3)c1</chem>	54.3	[14]
10		<chem>O=C(OC)[C@]12[N@@](Cc3c4c(c5c(c3C1)cc(OC)c(OC)c5)cc(OC)cc4)CCC2</chem>	53.8	[14]
11		<chem>O(C)c1c(OC)cc2c(c3c(c4c2C[C@]2(CO)[N@@](C4)CCC2)ccc(OC)c3)c1</chem>	85.3	[14]
12		<chem>O(C)c1c(OC)cc2c(c3c(c4c2C[C@]2(C)[N@@](C4)CCC2)ccc(OC)c3)c1</chem>	55.5	[14]
13		<chem>O(C)c1c(OC)cc2c(c3c(c4c2[C@@H](O)[C@]2(C)[N@@](C4)CCC2)ccc(OC)c3)c1</chem>	63.8	[14]
14		<chem>O(C)c1c(OC)cc2c(c3c(c4c2C[N@@]2[C@H](C4)CCC2)ccc(OC)c3)c1</chem>	71.2	[31]
15		<chem>O(C)c1c(OC)cc2c(c3c(c4c2NC[C@H]2[N@@](C4)CCC2)cc(OC)c(OC)c3)c1</chem>	40.4	[31]

Table 1. Cont.

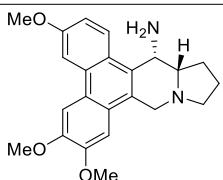
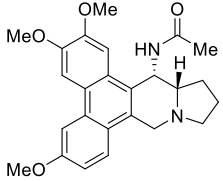
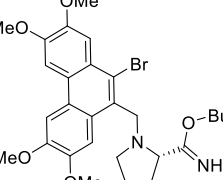
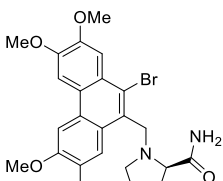
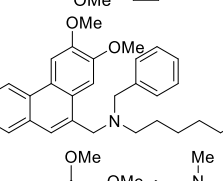
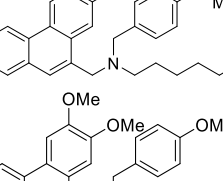
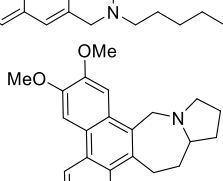
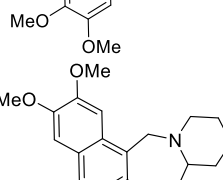
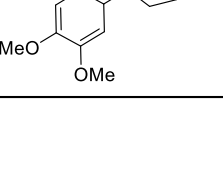
Compd	Structure	Smiles	Inhibition Rate (%)	Ref
16		<chem>O(C)c1c(OC)cc2c(c3c(c4[C@H](N)[C@H]5[N@@](Cc24)CCC5)ccc(OC)c3)c1</chem>	72.4	[27]
17		<chem>O=C(N[C@@H]1[C@H]2[N@@](Cc3c4c(c5c(c13)cc(OC)c(OC)c5)cc(OC)cc4)CCC2)C</chem>	75.1	[27]
18		<chem>BrC1c(C[N@@]2[C@H](C(OC(C)(C)C)=N)CCC2)c2c(c3c1cc(OC)c(OC)c3)cc(OC)c(OC)c2</chem>	39.7	[26]
19		<chem>BrC1c(C[N@@]2[C@@H](C(=O)N)CCC2)c2c(c3c1cc(OC)c(OC)c3)cc(OC)c(OC)c2</chem>	44.3	[26]
20		<chem>O=C(OC)CCCCC[N@](Cc1c2c(c3c(cc(OC)c(OC)c3)c1)cc(OC)c(OC)c2)Cc1cccc1</chem>	57.6	[24]
21		<chem>O=C(OC)CCCCC[N@](Cc1c2c(c3c(cc(OC)c(OC)c3)c1)cc(OC)c(OC)c2)Cc1ccc(N(C)C)cc1</chem>	55.3	[24]
22		<chem>O=C(OC)CCCCC[N@](Cc1c2c(c3c(cc(OC)c(OC)c3)c1)cc(OC)c(OC)c2)Cc1ccc(OC)cc1</chem>	50.0	[24]
23		<chem>O(C)c1c(OC)cc2c(c3c(c4c2C[N@@]2[C@@H](CC4)CC2)cc(OC)c(OC)c3)c1</chem>	43.8	[9]
24		<chem>O(C)c1c(OC)cc2c(c3c(c4c2C[N@@]2[C@@H](CC4)CCCC2)cc(OC)c(OC)c3)c1</chem>	54.7	[9]

Table 1. Cont.

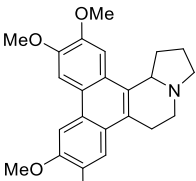
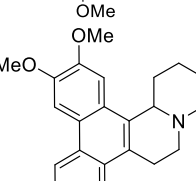
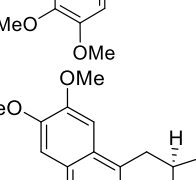
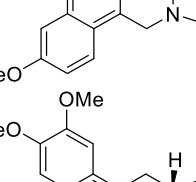
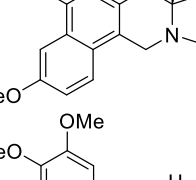
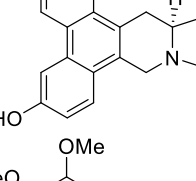
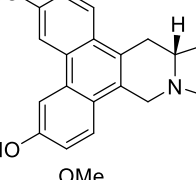
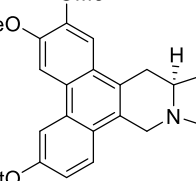
Compd	Structure	Smiles	Inhibition Rate (%)	Ref
25		<chem>O(C)c1c(OC)cc2c(c3c(c4c2[C@@H]2[N@](CC4)CCC2)cc(OC)c(OC)c3)c1</chem>	60.0	[9]
26		<chem>O(C)c1c(OC)cc2c(c3c(c4c2[C@H]2[N@](CC4)CCCC2)cc(OC)c(OC)c3)c1</chem>	37.7	[9]
27		<chem>O(C)c1c(OC)cc2c(c3c(c4c2C[C@@H]2[N@@](C4)CCC2)ccc(OC)c3)c1</chem>	65.8	[25]
28		<chem>O(C)c1c(OC)cc2c(c3c(c4c2C[C@H]2[N@@](C4)CCC2)ccc(OC)c3)c1</chem>	60.2	[25]
29		<chem>O(C)c1c(OC)cc2c(c3c(c4c2C[C@@H]2[N@@](C4)CCC2)ccc(O)c3)c1</chem>	70.5	[25]
30		<chem>O(C)c1c(OC)cc2c(c3c(c4c2C[C@H]2[N@@](C4)CCC2)ccc(O)c3)c1</chem>	52.2	[25]
31		<chem>O(CC)c1cc2c3c(c4c(c2cc1)C[N@@]1[C@@H](C4)CCC1)cc(OC)c(OC)c3</chem>	50.0	[25]
32		<chem>O(CC)c1cc2c3c(c4c(c2cc1)C[N@@]1[C@H](C4)CCC1)cc(OC)c(OC)c3</chem>	56.2	[25]

Table 1. Cont.

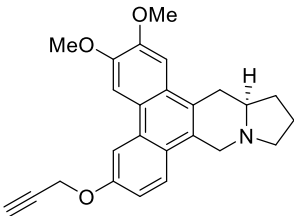
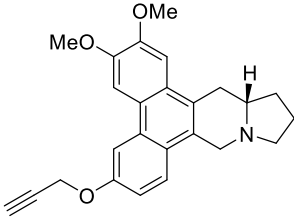
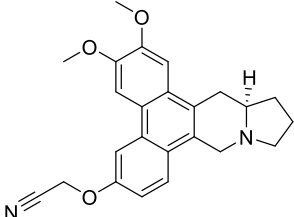
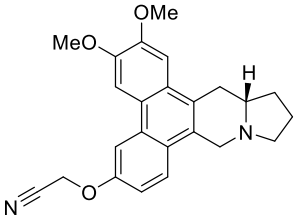
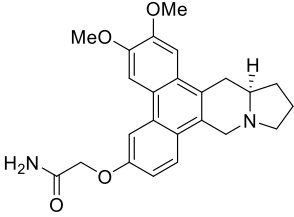
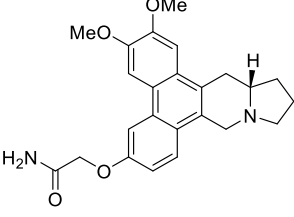
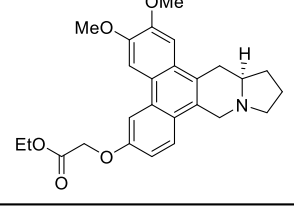
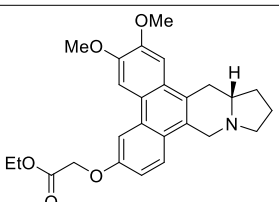
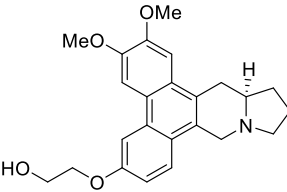
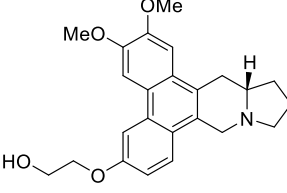
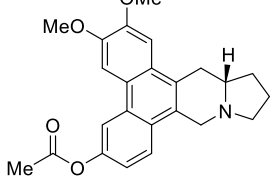
Compd	Structure	Smiles	Inhibition Rate (%)	Ref
33		<chem>O(CC#C)c1cc2c3c(c4c(c2cc1)C[N@@]1[C@@H](C4)CCC1)cc(OC)c(OC)c3</chem>	61.2	[25]
34		<chem>O(CC#C)c1cc2c3c(c4c(c2cc1)C[N@@]1[C@H](C4)CCC1)cc(OC)c(OC)c3</chem>	75.0	[25]
35		<chem>O(CC#N)c1cc2c3c(c4c(c2cc1)C[N@@]1[C@@H](C4)CCC1)cc(OC)c(OC)c3</chem>	79.3	[25]
36		<chem>O(CC#N)c1cc2c3c(c4c(c2cc1)C[N@@]1[C@H](C4)CCC1)cc(OC)c(OC)c3</chem>	60.0	[25]
37		<chem>O=C(N)COc1cc2c3c(c4c(c2cc1)C[N@@]1[C@@H](C4)CCC1)cc(OC)c(OC)c3</chem>	78.5	[25]
38		<chem>O=C(N)COc1cc2c3c(c4c(c2cc1)C[N@@]1[C@H](C4)CCC1)cc(OC)c(OC)c3</chem>	52.3	[25]
39		<chem>O=C(OCC)COc1cc2c3c(c4c(c2cc1)C[N@@]1[C@@H](C4)CCC1)cc(OC)c(OC)c3</chem>	74.6	[25]

Table 1. Cont.

Compd	Structure	Smiles	Inhibition Rate (%)	Ref
40		<chem>O=C(OCC)COc1cc2c3c(c4c(c2cc1)C[N@@]1[C@H](C4)CCC1)cc(OC)c(OC)c3</chem>	50.4	[25]
41		<chem>O(CCO)c1cc2c3c(c4c(c2cc1)C[N@@]1[C@@H](C4)CCC1)cc(OC)c(OC)c3</chem>	78.2	[25]
42		<chem>O(CCO)c1cc2c3c(c4c(c2cc1)C[N@@]1[C@H](C4)CCC1)cc(OC)c(OC)c3</chem>	43.9	[25]
43		<chem>O=C(Oc1cc2c3c(c4c(c2cc1)C[N@@]1[C@H](C4)CCC1)cc(OC)c(OC)c3)C</chem>	68.7	[25]

2. Materials and Methods

2.1. Molecule Library Preparation

The inhibition rates (%) of 43 compounds of antofine analogue including ningenmycin (1) and ribavirin (2) ($500 \mu\text{g mL}^{-1}$) under investigation against TMV were collected from the literature [9,14,24–27,31] and are summarized in Table 1 along with their smiles. Compounds 1–43 had the highest anti-TMV activities in these studies, with anti-TMV activities ranging from 38 to 85 g mL^{-1} . The structures of the compounds involved in the current study were optimized, and their global reactivity descriptors were estimated using the density functional theory (DFT) method with the B3LYP/6-31G basis set through the Gaussian 09 [32,34]. The convergent value of maximum force, root-mean-square (RMS) force, maximum displacement, and RMS displacement were set by default and achieved “YES”. All the values were positive after the calculation of the vibrational frequencies of the compounds. The results indicated that the 43 compounds have stable confirmations. The affinity of the optimized structures was investigated using the MOE software [33]. The simulations were performed several times and the variations were marginal.

2.2. Receptor Preparation

The accumulation of TMV coat protein (CP) within chloroplasts can influence photosynthesis in infected plants by inhibiting photosystem II [35]. Likewise, in TMV replication, one or more of the viral proteins direct the assembly of virus replication complexes (VRCs) in association with the host-derived membranes [36]. The CP improves the movement of protein (MP), increases the VRC size, and facilitates the replication and spread of the TMV [37]. TMV-CP was considered to be an initiating viral assembly. Therefore, the TMV-CP was selected as an important binding site for antiviral agents. The three-dimensional crystal structure of TMV-CP (PDB ID: 2OM3) [38] was downloaded from the Research Collaboratory for Structural Bioinformatics (RCSB) Protein Data Bank (PDB) database [39].

The receptor protein was prepared by leaving water (solvent) molecules within the active site to ensure the formation of a hydrogen bond between the ligand and the target using the MOE software. The missing bonds in the protein structure, which were broken through X-ray diffraction, were corrected, and the protein was protonated. Following optimization using the assisted model building and energy refinement (Amber 10): Extended Hückel Theory (EHT) force, the molecular docking of the TMV-CP with the selected compounds was conducted [40].

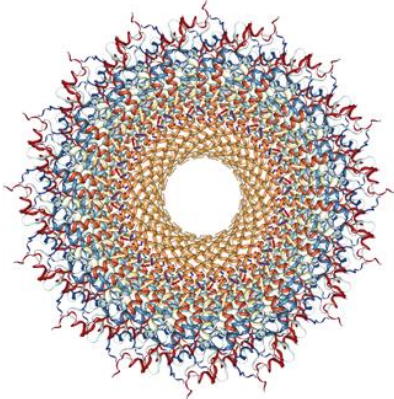
2.3. Global Reactivity Descriptors

The correlation between specific theoretical parameters and the inhibitive performance of the antofine analogues were investigated *in silico*. Therefore, some of the molecular properties of the antofine analogues that describe the global reactivity were calculated using the Gaussian 09 software at B3LYP/6-31G [32]. The parameters calculated were the highest occupied molecular orbital energy (E_{HOMO}), the lowest unoccupied molecular orbital energy (E_{LUMO}), the energy gap ($\Delta E = E_{\text{LUMO}} - E_{\text{HOMO}}$), the global electrophilicity index ($\omega = \mu^2/2\eta$), the chemical potential ($\mu = [E_{\text{LUMO}} + E_{\text{HOMO}}]/2$), the chemical hardness ($\eta = [E_{\text{LUMO}} - E_{\text{HOMO}}]/2$), the chemical softness ($s = 1/2\eta$), the nucleophilicity ($N = E_{\text{HOMO}}(\text{Nucleophile}) - E_{\text{HOMO}}(\text{tetracyanoethylene, TCE})$), the ionization potential ($\text{IP} = -E_{\text{HOMO}}$), and the electron affinity ($\text{EA} = -E_{\text{LUMO}}$) [41].

2.4. Molecular Docking

The MOE software [33] was used to perform molecular docking and scoring calculations. The resolution for the crystal structure of the TMV-CP (PDB ID: 2OM3) was 4.4 Å. The receptors were selected as rigid and ligands as flexible for the docking simulation. The root-mean-square distance (RMSD) in the range of 1.5–3.0 and the energy score of ca. -7 Kcal/mol were considered as the criteria for the result obtained from the molecular docking [42,43]. Details of the three-dimensional crystal structure (2OM3) of TMV-CP are shown in Table 2.

Table 2. Details of the three-dimensional crystal structure (PDB ID: 2OM3) of TMV-CP.

	TMV-CP	3D Structure of TMV-CP
Code	2OM3	
Method	Electron Microscopy	
Resolution	4.40 Å	
Number of residues	158	

The binding site residues used as inputs for receptor grid generation during induced-fit docking included Gln36, Thr37, Gln38, Arg41, Thr42, Gln45, Arg46, Phe87, Asp88, Thr89, Arg90, Asn91, Arg92, Glu95, and Val114.

2.5. Molecular Dynamics Simulations

The Nosé–Poincaré–Andersen (NPA) method is a real-time Hamiltonian formulation of isothermal–isobaric molecular dynamics simulation based on a Poincaré time transformation of the Nosé–Andersen Hamiltonian [44]. It was used to evaluate the MD of ligands [44]. The optimized system setting included the use of the MMFF94x force field, sphere shape, water as a solvent, six margins, and deletion of the existing solvent with a distance of more than

4 Å. During the NPA calculations, the system was equilibrated at 300 K for 100 ps then run for 1500 ps with the time steps 0.002, and the constraints were applied on light bonds.

3. Results and Discussion

3.1. Global Reactivity Descriptors

Analysis of density functional theory descriptors gives more information about the characteristics of stability, electrophilicity, and nucleophilicity of the compounds. Therefore, the global reactivity descriptors were calculated for the 43 compounds under investigation using the DFT method with the B3LYP/6-31G basis set. The results obtained are summarized in Table 3.

Table 3. The HOMO and LUMO energy, energy gap (ΔE), and reactivity indices (η , S, μ , ω , and N) of the 43 compounds under investigation.

Compd	HOMO (eV)	LUMO (eV)	ΔE (eV) ^a	η (eV) ^a	S	μ	ω (eV)	N (eV)
1	-6.38	-1.63	4.75	2.37	155.96	-4.00	3.38	2.28
2	-6.96	-1.29	5.66	2.83	130.71	-4.12	3.00	1.70
3	-5.23	-0.72	4.51	2.25	164.20	-2.97	1.96	3.43
4	-5.31	-0.86	4.45	2.23	166.34	-3.08	2.14	3.35
5	-5.27	-0.81	4.46	2.23	166.05	-3.04	2.07	3.38
6	-5.04	-0.93	4.11	2.06	180.08	-2.99	2.17	3.61
7	-5.21	-0.67	4.54	2.27	163.26	-2.94	1.91	3.45
8	-5.38	-0.88	4.50	2.25	164.66	-3.13	2.17	3.28
9	-5.50	-0.96	4.54	2.27	163.25	-3.23	2.30	3.16
10	-5.17	-0.78	4.40	2.20	168.38	-2.98	2.01	3.49
11	-5.10	-0.84	4.26	2.13	173.79	-2.97	2.07	3.55
12	-5.17	-0.71	4.46	2.23	166.14	-2.94	1.94	3.49
13	-5.32	-0.85	4.46	2.23	165.86	-3.08	2.13	3.34
14	-5.16	-0.75	4.41	2.21	167.83	-2.95	1.97	3.50
15	-5.10	-0.87	4.24	2.12	174.80	-2.99	2.10	3.55
16	-5.21	-0.79	4.42	2.21	167.42	-3.00	2.04	3.44
17	-5.55	-1.11	4.44	2.22	166.64	-3.33	2.50	3.10
18	-5.37	-1.03	4.34	2.17	170.47	-3.20	2.36	3.28
19	-5.52	-1.51	4.02	2.01	184.41	-3.51	3.08	3.13
20	-5.52	-1.02	4.50	2.25	164.46	-3.27	2.37	3.14
21	-4.94	-0.87	4.06	2.03	182.20	-2.90	2.07	3.72
22	-5.55	-0.96	4.60	2.30	161.10	-3.25	2.30	3.10
23	-5.34	-0.92	4.42	2.21	167.58	-3.13	2.22	3.32
24	-5.39	-0.93	4.45	2.23	166.23	-3.16	2.24	3.27
25	-5.50	-0.93	4.56	2.28	162.22	-3.22	2.27	3.16
26	-5.30	-0.94	4.36	2.18	169.81	-3.12	2.23	3.36
27	-5.27	-0.84	4.43	2.21	167.17	-3.06	2.11	3.39
28	-5.37	-0.82	4.54	2.27	163.00	-3.09	2.11	3.29
29	-5.39	-0.87	4.52	2.26	163.96	-3.13	2.17	3.27
30	-5.42	-0.90	4.53	2.26	163.59	-3.16	2.21	3.23
31	-5.25	-0.82	4.42	2.21	167.35	-3.03	2.08	3.41
32	-5.29	-0.84	4.45	2.22	166.48	-3.06	2.11	3.37
33	-5.34	-0.91	4.43	2.21	167.17	-3.13	2.21	3.31
34	-5.38	-0.93	4.45	2.22	166.43	-3.16	2.24	3.28
35	-5.55	-1.13	4.42	2.21	167.47	-3.34	2.53	3.10
36	-5.57	-1.15	4.42	2.21	167.52	-3.36	2.55	3.09
37	-5.51	-1.07	4.44	2.22	166.74	-3.29	2.44	3.15
38	-5.53	-1.09	4.44	2.22	166.72	-3.31	2.46	3.13
39	-5.29	-0.83	4.46	2.23	166.03	-3.06	2.10	3.37
40	-5.38	-0.93	4.45	2.22	166.43	-3.16	2.24	3.28
41	-5.34	-0.90	4.44	2.22	166.69	-3.12	2.20	3.31
42	-5.42	-0.88	4.55	2.27	162.85	-3.15	2.18	3.23
43	-5.65	-1.26	4.39	2.20	168.54	-3.45	2.71	3.01

Note: ΔE : energy gap, η : chemical hardness, S: chemical softness, μ : chemical potential, ω : electrophilicity, and N: nucleophilicity.

Table 3 shows that all compounds have a similar trend in all descriptors except for **21** and the reference compounds **1** and **2**. Affinity ($A = -E_{\text{LUMO}}$) and potential ionization ($I = -E_{\text{HOMO}}$) are related to one-electron orbital energies of HOMO and LUMO, respectively. They can be used to measure electronegativity and hardness. Compound **21** has the lowest potential ionization (4.94 eV) while the reference compounds **1** and **2** have the larger affinity (1.63 eV and 1.29 eV, respectively). Therefore, compound **21** acts as a good electron donor (the strongest nucleophile, $N = 3.80$ eV) while the reference compounds **1** and **2** act as good electron acceptors (the strongest electrophiles; $\omega = 3.38$ and 3.00 eV, respectively).

The ΔE is used to measure the chemical reactivity and the kinetic stability of molecules. A large ΔE gap indicates high kinetic stability, low reactivity, and a poorly polarizable molecule (i.e., a weak reactivity). The lowest ΔE value was observed for compounds **19** and **21** (4.02 and 4.06 eV, respectively), and the highest ΔE was seen for the reference compounds **1** and **2** (4.75 and 5.67 eV, respectively). Such a result indicates that compounds **19** and **21** are highly polarizable and therefore develop a high reactivity. The high chemical hardness and low chemical softness are indicators of the overall stability of the system. The lowest η was observed for compounds **19** and **21** (2.01 and 2.03 eV, respectively), while the reference compounds **1** and **2** showed the highest chemical hardness as 2.37 and 2.83 eV, respectively. On the other hand, compounds **19** and **21** showed the highest chemical softness ($S = 184.41$ and 182.20), and the reference compounds **1** and **2** showed the smallest S values (155.96 and 130.71, respectively). Clearly, compounds **19** and **21** are the softest and most reactive molecules compared to the others.

The electronic chemical potential (μ) reflects the charge transfer from a system with a high electronic chemical potential to another with a lower μ . Compound **21** has the highest μ (−2.90 eV), while the references **1** and **2** have the lowest values as −4.00 eV and −4.12 eV, respectively. According to these results, **21** can exchange electron density with the environment efficiently and better than other compounds.

In terms of nucleophilicity, organic molecules can be classified as strong ($N > 3$ eV), moderate ($2.0 \text{ eV} \leq N \leq 3.0 \text{ eV}$), and marginal nucleophiles ($N < 2.0 \text{ eV}$) [41,45]. The biological activity of the antofine analogues can be predicted using the electrophilicity (ω) and nucleophilicity (N) indexes. In addition, electrophilicity (ω) provides important information about the reactivity of organic compounds that are involved in polar reactions ($\omega > 2.0 \text{ eV}$) [41,45]. The results obtained indicated that compound **21** ($N = 3.72 \text{ eV}$) is the strongest nucleophile, while the reference compounds **1** and **2** ($\omega = 3.38$ and 3.00 eV, respectively) are the strongest electrophiles.

3.2. Molecular Docking

The 43 selected compounds were docked into the binding site of the TMV-CP (PDB ID: 2OM3) to assess their abilities to inhibit the disease caused by the virus. The results obtained are summarized in Table 4.

The molecular docking score of the 43 compounds varied from −5.29 to −7.93 kcal/mol, and the RMSD ranged between 0.71 and 2.83 Å. The ligand binds best with a specific receptor when RMSD is close to 2 Å with an energy score that ≤ -7 kcal/mol [42,43]. These two values were used as criteria to validate the molecular docking results. Table 5 shows the results obtained for only the compounds that gave valid molecular docking scores.

Table 4. Molecular docking score and RMSD of the 43 compounds under investigation.

Compd	Score (kcal/mol)	RMSD (Å)	Compd	Score (kcal/mol)	RMSD (Å)
1	−6.98	2.83	25	−6.25	1.36
2	−5.29	2.07	26	−6.39	1.70
3	−6.30	1.21	23	−6.59	1.96
4	−6.16	1.43	24	−6.60	1.72
5	−6.73	1.03	27	−6.41	0.71
6	−6.41	2.05	28	−6.05	1.50
7	−6.07	1.24	29	−6.30	1.52
8	−6.40	1.16	30	−5.86	1.89
9	−6.24	2.04	31	−6.49	1.26
10	−6.18	1.67	32	−6.35	1.59
11	−6.28	2.27	33	−6.72	0.71
12	−6.26	1.34	34	−6.71	1.63
13	−6.08	2.43	35	−6.49	1.59
14	−6.28	1.22	36	−6.59	1.01
15	−6.65	1.66	37	−6.70	1.08
16	−6.39	1.41	38	−6.58	1.91
17	−6.37	1.90	39	−7.07	1.66
18	−6.72	1.64	40	−6.72	2.78
19	−6.66	1.51	41	−6.40	1.22
20	−6.73	2.30	42	−6.32	1.67
21	−7.93	2.37	43	−6.23	1.52
22	−7.25	2.31			

Table 5. Molecular docking score, RMSD, and binding affinity for the compounds showed valid molecular docking scores with 2OM3.

Compd	Score (kcal/mol)	RMSD (Å)	Bonds between Atoms of Compounds and Residues of Active Site of 2OM3						
			Compd Atoms	Receptor Atoms	Receptor Residues	Interaction	d (Å)	E (kcal/mol)	Total E (kcal/mol)
1	−6.98	2.83	N	OG1	Thr42	H—D	3.01	−0.8	−37.59
			O	OE1	Gln38	H—D	2.80	−2.1	
			O	NH2	Arg90	H—A	3.08	−2.7	
			N	NH1	Arg90	H—A	3.00	−2.3	
2	−5.29	2.07	O	OE1	Gln38	H—D	2.86	−2.3	−26.92
			O	N	Asn91	H—A	3.16	−1.9	
3	−6.30	1.21	—	—	—	—	—	−31.46	
4	−6.16	1.43	—	—	—	—	—	−31.92	
6	−6.41	2.05	6-ring	NH1	Arg92	π -cation	3.52	−1.1	−33.66
17	−6.37	1.90	O	N	Asn91	H—A	3.11	−1.3	−32.72
18	−6.72	1.64	N	NH2	Arg90	H—A	3.15	−5.4	−36.16
19	−6.66	1.51	N	OE1	Gln38	H—D	3.26	−1.0	−34.24
			O	N	Asn91	H—A	3.19	−1.0	
20	−6.73	2.30	—	—	—	—	—	−32.50	
21	−7.93	2.37	O	NE	Arg92	H—A	3.14	−3.0	−44.72
			O	NH2	Arg92	H—A	3.01	−2.3	
			O	NH2	Arg90	H—A	2.92	−1.2	
			N	NH2	Arg90	H—A	3.31	−2.3	
22	−7.25	2.32	O	NE	Arg92	H—A	3.00	−3.7	−39.90
			O	NH2	Arg92	H—A	3.20	−0.8	
			O	NH2	Arg90	H—A	3.02	−1.3	
23	−6.59	1.96	N	NH2	Arg90	H—A	3.26	−2.0	−35.28
24	−6.60	1.72	O	N	Asn91	H—A	3.13	−1.3	−35.19
38	−6.58	1.91	N	OD1	Asn91	H—D	2.87	−4.5	−33.62

d: distance, H—D: hydrogen doner, and H—A: hydrogen acceptor.

Compounds **1**, **21**, and **22** showed the highest docking scores of -6.98 , -7.93 , and -7.25 kcal/mol, respectively (i.e., they have the highest inhibitory potential). Compound **21** docked with a binding affinity of -44.72 kcal/mol, which is the highest compared with the others and interacted with Arg90 and Arg92. Compound **22** docked with a binding affinity of -39.90 kcal/mol and interacted with Arg90 and Arg92. Compound **1** docked with a binding affinity of -37.59 kcal/mol and interacted with Thr42, Gln38, and Arg90. The docking binding affinities were lower for the other compounds.

Compounds **20–22** have similar structures since they contain esters and long-chain alkyl groups but have different substituents on benzyl rings. However, they had different binding affinities. Compound **20** gave the lowest binding affinity among the three compounds. It seems that the effect of the donor groups NMe_2 and OCH_3 , attached at the *para* position of the benzyl moiety within the skeleton of the molecules, caused **21** and **22** to interact more significantly. Figure 1 represents the interactions of compounds **1** and **20–22** with 2OM3.

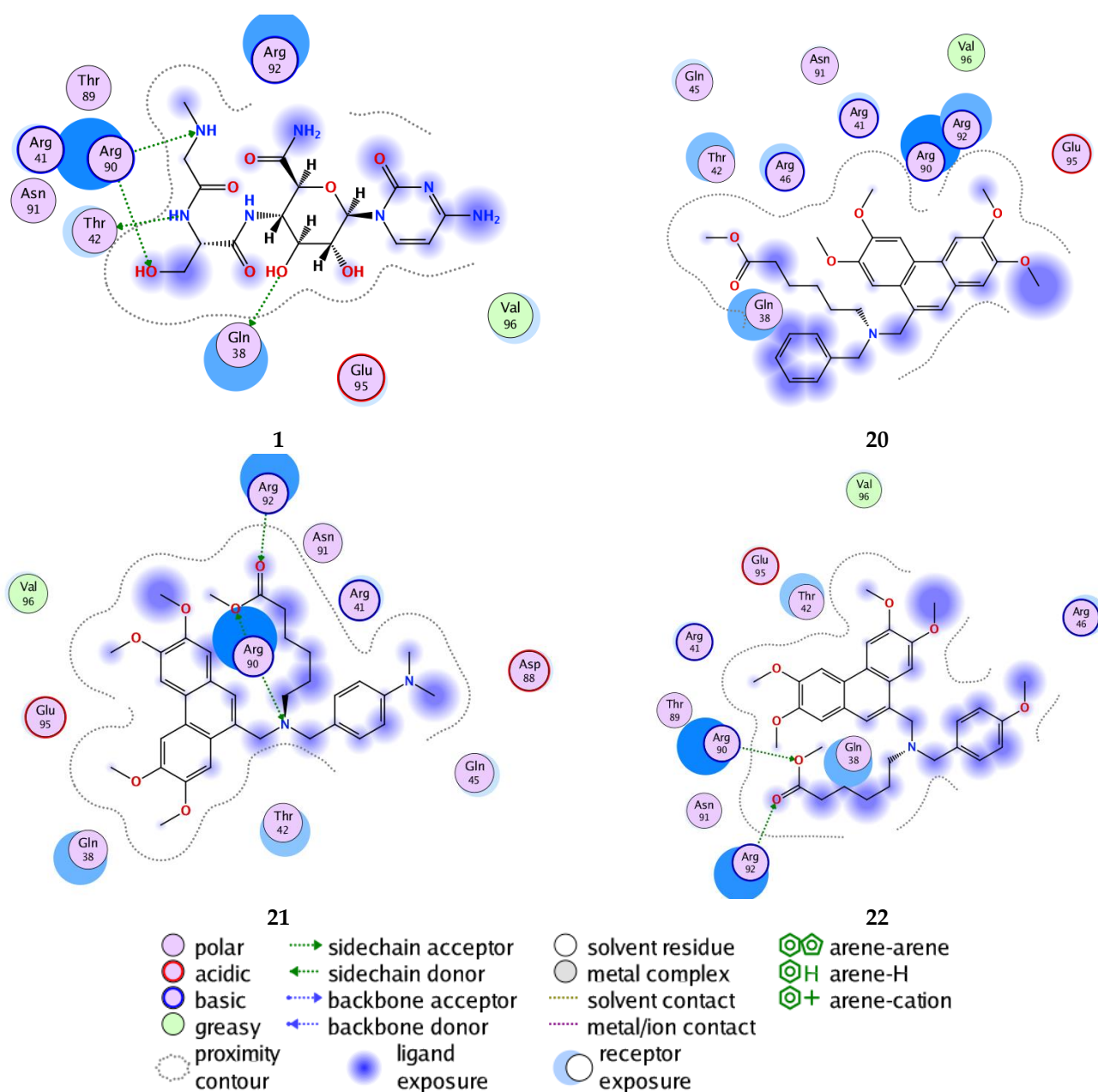


Figure 1. Binding affinity of compounds **1** and **20–22** with 2OM3.

3.3. Molecular Dynamics Simulations

The stability and dependable binding affinities of the docked receptor-ligand complexes of the top four promising inhibitors, namely, compounds **1** and **20–22**, were analyzed further using the MD simulations. Figure 2 shows the stability of the four receptor-ligand complexes with time. The four complexes showed the same trends and were stable in the simulation process during the same period of time and fluctuated between 0 and 1500 s before they stabilized.

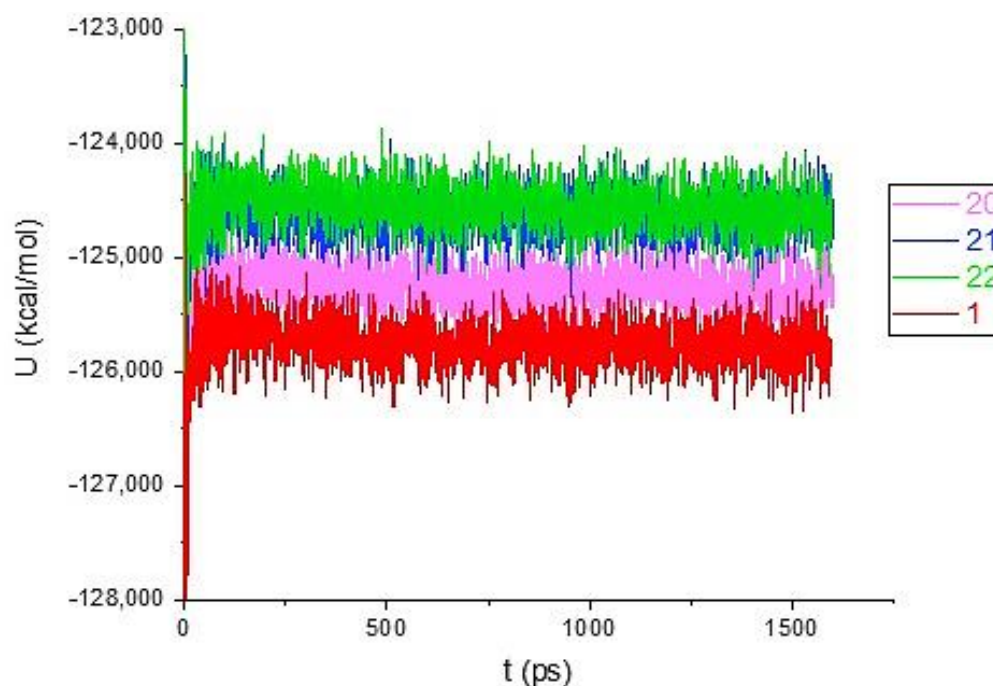


Figure 2. The evaluation of potential energy of complexes of **1** and **20–22** with 2OM3 receptor as a function of time.

Binding Free Energy Calculations

In the molecular mechanics generalized born surface area (MM/GBSA) calculations, the affinity of one inhibitor binding to the receptor could be estimated using the snapshots from a trajectory of the complex. The absolute binding free energies of **1** and **20–22**, using the MM/GBSA technique, are shown in Table 6.

Table 6. Calculated MM-GBSA binding energies (kcal/mol) for compounds **1** and **20–22** against 2OM3 over MD simulations.

Compd	MM-GBSA
1	−42.14
20	−19.95
21	−33.71
22	−49.95

Compound **20** showed a relatively weak binding energy compared to the others. The reported anti-TMV activities of compounds **1** and **20–22** were 69.3, 57.6, 55.3, and 50.0%, respectively (Table 1). Clearly, the predicted binding free energy of these four compounds was in good agreement with the inhibition results. Compound **22** showed a great binding energy, while **1** and **21** showed moderate binding energy.

Generally, the molecular recognition of the ligand is important if the interaction energy between a residue and a ligand is lower than -0.8 kcal/mol [46]. Compound **1** has a favorable energy contribution (-1.5 to -3.1 kcal/mol) originating predominately from a

Glu95 H-donor (-3.1 and -1.5 kcal/mol), whereas the other energy contributions originate from an H₂O H-donor (-0.3 to -2.3 kcal/mol) and H-acceptor (-1.1 to -2.2 kcal/mol).

Figure 3 shows that compound **22** has a favorable energy contribution of -1.6 to -1.9 kcal/mol, which originates predominately from an Arg90 and Thr42 by an H₂O through H-acceptor (-1.9 and -1.6 kcal/mol). Compound **21** has interactions with an Asp88 and Thr89 by an H₂O through H-acceptor (-0.9 and -1.8 kcal/mol). Compound **20** has interactions with an Asn91 through H-acceptor (-1.4 kcal/mol) and an H₂O through H-acceptor (-0.9 kcal/mol) and pi-H (-1.4 kcal/mol).

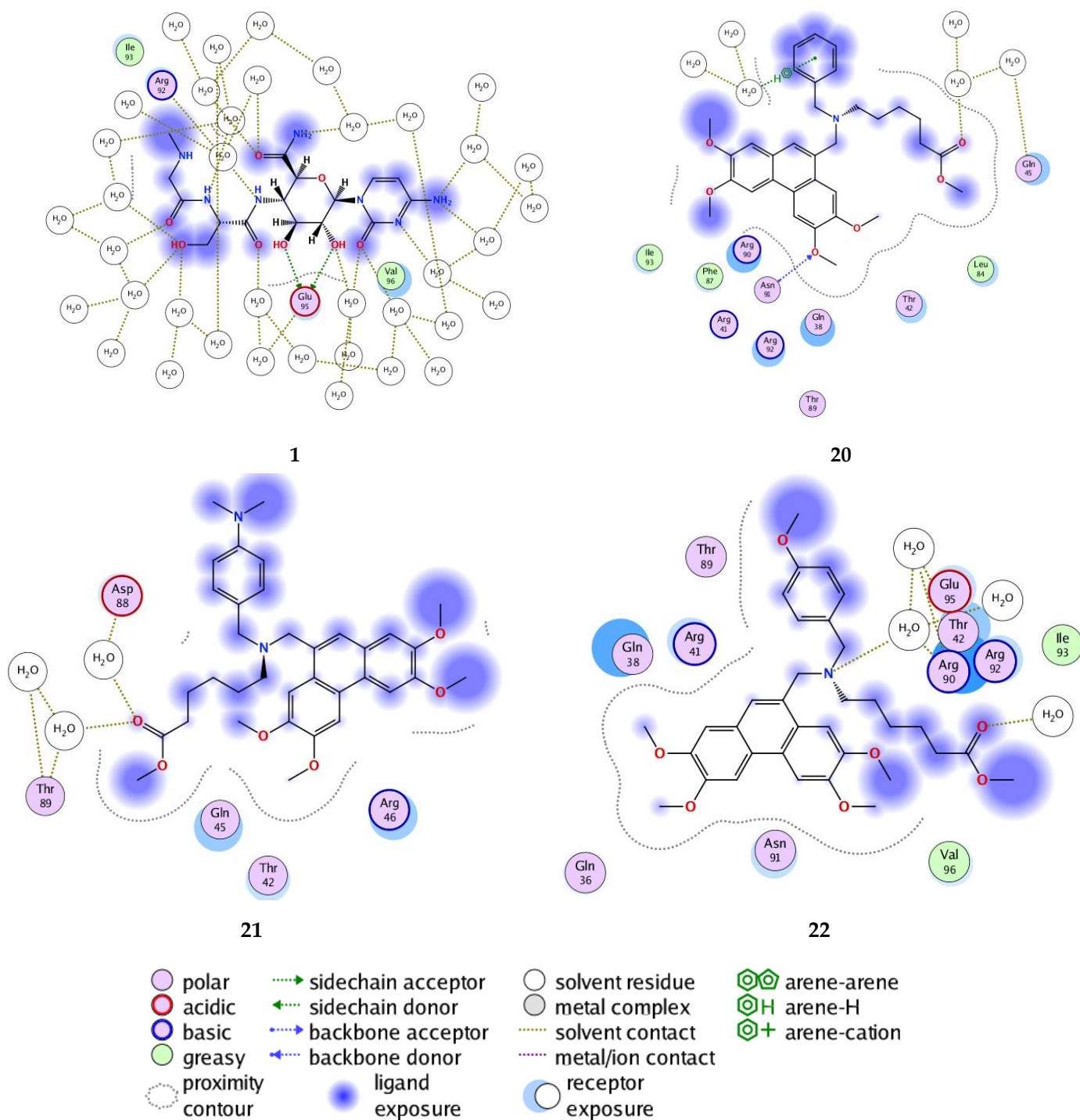


Figure 3. Docked pose and binding affinity of compounds **1** and **20–22**.

On the basis of the analysis performed, it appears that compound **21** interacted strongly with the 2OM3 mainly through an Asp88 and Thr89, whereas compound **22** interacted with 2OM3 through an Arg90 and Thr42. However, compound **20** has a single interaction with the 2OM3 through an Asn91.

4. Conclusions

The *in silico* anti-tobacco mosaic virus activity of 43 antofine analogues was assessed. The docking results showed that compounds **20–22** that contain an ester group gave the lowest energy score and good root-mean-square distance. These compounds showed good binding results, particularly the ones containing an ester unit and a long-chain alkyl groups along with an electron-donating substituent on benzyl moiety. These functional groups facilitate the interaction with the active site of the tobacco mosaic virus coat protein (2OM3).

Author Contributions: Conceptualization and experimental design: H.A.A., B.A.S., D.H. and H.K.; experimental work and data analysis: validation, B.A.S., N.L.H. and G.A.E.-H.; writing—original draft preparation: H.A.A., B.A.S., D.H., B.A.S., N.L.H. and G.A.E.-H.; writing—review and editing B.A.S., N.L.H. and G.A.E.-H. All authors have read and agreed to the published version of the manuscript.

Funding: The research was funded by the Researchers Supporting Project number (RSP-2021/404), King Saud University, Riyadh, Saudi Arabia.

Institutional Review Board Statement: Not applicable.

Informed Consent Statement: Not applicable.

Data Availability Statement: Data are contained within the article.

Acknowledgments: H.K. and D.H. thank the University of Biskra and B.A.S. thanks the University of Basrah for their support.

Conflicts of Interest: The authors declare no conflict of interest. The funders had no role in the design of the study; in the collection, analyses, or interpretation of data; in the writing of the manuscript, or in the decision to publish the results.

References

1. Rubio, L.; Galipienso, L.; Ferriol, I. Detection of plant viruses and disease management: Relevance of genetic diversity and evolution. *Front. Plant Sci.* **2020**, *11*, 1092. [[CrossRef](#)] [[PubMed](#)]
2. Nazarov, P.A.; Baleev, D.N.; Ivanova, M.I.; Sokolova, L.M.; Karakozova, M.V. Infectious plant diseases: Etiology, current status, problems and prospects in plant protection. *Acta Nat.* **2020**, *12*, 46–59. [[CrossRef](#)] [[PubMed](#)]
3. Mehetre, G.T.; Leo, V.V.; Singh, G.; Sorokan, A.; Maksimov, I.; Yadav, M.K.; Upadhyaya, K.; Hashem, A.; Alsaleh, A.N.; Dawoud, T.M.; et al. Current developments and challenges in plant viral diagnostics: A systematic review. *Viruses* **2021**, *13*, 412. [[CrossRef](#)] [[PubMed](#)]
4. Jones, R.A.C. Global plant virus disease pandemics and epidemics. *Plants* **2021**, *10*, 233. [[CrossRef](#)]
5. Lomonosoff, G.P.; Wege, C. TMV Particles: The journey from fundamental studies to bionanotechnology applications. *Adv. Virus Res.* **2018**, *102*, 149–176. [[CrossRef](#)]
6. Knapp, E.; Lewandowski, D.J. Tobacco mosaic virus, not just a single component virus anymore. *Mol. Plant Pathol.* **2001**, *2*, 117–123. [[CrossRef](#)]
7. Adams, M.J.; Adkins, S.; Bragard, C.; Gilmer, D.; Li, D.; MacFarlane, S.A.; Wong, S.-M.; Melcher, U.; Ratti, C.; Ryu, K.H.; et al. ICTV Virus taxonomy profile: *Virgaviridae*. *J. Gen. Virol.* **2017**, *98*, 1999–2000. [[CrossRef](#)]
8. Lv, X.; Xiang, S.; Wang, X.; Wu, L.; Liu, C.; Yuan, M.; Gong, W.; Win, H.; Hao, C.; Xue, Y.; et al. Synthetic chloroinconazole compound exhibits highly efficient antiviral activity against tobacco mosaic virus. *Pest. Manag. Sci.* **2020**, *76*, 3636–3648. [[CrossRef](#)]
9. Su, B.; Chen, F.; Wang, L.; Wang, Q. Design, synthesis, antiviral activity, and structure–activity relationships (SARs) of two types of structurally novel phenanthroindole/quinolizidine analogues. *J. Agric. Food Chem.* **2014**, *62*, 1233–1239. [[CrossRef](#)]
10. Zhao, L.; Feng, C.H.; Hou, C.T.; Hu, L.Y.; Wang, Q.C.; Wu, Y.F. First discovery of acetone extract from cottonseed oil sludge as a novel antiviral agent against plant viruses. *PLoS ONE* **2015**, *10*, e0117496. [[CrossRef](#)]
11. Gan, X.H.; Hu, D.Y.; Wang, Y.J.; Yu, L.; Song, B.A. Novel trans-ferulic acid derivatives containing a chalcone moiety as potential activator for plant resistance induction. *J. Agric. Food Chem.* **2017**, *65*, 4367–4377. [[CrossRef](#)] [[PubMed](#)]
12. Lu, A.; Wang, T.; Hui, H.; Wei, X.; Cui, W.; Zhou, C.; Li, H.; Wang, Z.; Guo, J.; Ma, D.; et al. Natural products for drug discovery: Discovery of gramines as novel agents against a plant virus. *J. Agric. Food Chem.* **2019**, *67*, 2148–2156. [[CrossRef](#)] [[PubMed](#)]

13. Loustaud-Ratti, V.; Debette-Gratien, M.; Jacques, J.; Alain, S.; Marquet, P.; Sautereau, D.; Rousseau, A.; Carrier, P. Ribavirin: Past, present and future. *World, J. Hepatol.* **2016**, *8*, 123–130. [[CrossRef](#)] [[PubMed](#)]
14. Su, B.; Cai, C.; Deng, M.; Wang, Q. Spatial configuration and three-dimensional conformation directed design, synthesis, antiviral activity, and structure–activity relationships of phenanthroindolizidine analogues. *J. Agric. Food Chem.* **2016**, *64*, 2039–2045. [[CrossRef](#)]
15. Sofy, A.R.; Sofy, M.R.; Hmed, A.A.; Dawoud, R.A.; Alnaggar, A.E.-A.M.; Soliman, A.M.; El-Dougdoug, N.K. Ameliorating the adverse effects of tomato mosaic Tobamovirus infecting tomato plants in Egypt by boosting immunity in tomato plants using zinc oxide nanoparticles. *Molecules* **2021**, *26*, 1337. [[CrossRef](#)]
16. Sofy, A.R.; Sofy, M.R.; Hmed, A.A.; Dawoud, R.A.; Refaey, E.E.; Mohamed, H.I.; El-Dougdoug, N.K. Molecular characterization of the alfalfa mosaic virus infecting *Solanum melongena* in Egypt and the control of its deleterious effects with melatonin and salicylic acid. *Plants* **2021**, *10*, 459. [[CrossRef](#)]
17. Song, P.; Yu, X.; Yang, W.; Wang, Q. Natural phytoalexin stilbene compound resveratrol and its derivatives as anti-tobacco mosaic virus and anti-phytopathogenic fungus agents. *Sci. Rep.* **2021**, *11*, 16509. [[CrossRef](#)]
18. Guo, W.; Xiang Lu, X.; Liu, B.; Yan, H.; Feng, J. Anti-TMV activity and mode of action of three alkaloids isolated from *Chelidonium majus*. *Pest. Manag. Sci.* **2021**, *77*, 510–517. [[CrossRef](#)]
19. Hu, Z.-X.; Zou, J.-B.; An, Q.; Yi, P.; Yuan, C.-M.; Gu, W.; Zhao, L.-H.; Hao, X.-J. Anti-tobacco mosaic virus (TMV) activity of chemical constituents from the seeds of *Sophora tonkinensis*. *J. Asian Nat. Prod. Res.* **2021**, *23*, 644–651. [[CrossRef](#)]
20. Zhao, L.; Chen, Y.; Wu, K.; Yan, H.; Hao, X.; Wu, Y. Application of fatty acids as antiviral agents against tobacco mosaic virus. *Pestic. Biochem. Physiol.* **2017**, *139*, 87–91. [[CrossRef](#)]
21. Chen, M.-H.; Chen, Z.; Song, B.-A.; Bhadury, P.S.; Yang, S.; Cai, X.-J.; Hu, D.-Y.; Xue, W.; Zeng, S. Synthesis and antiviral activities of chiral thiourea derivatives containing an α -aminophosphonate moiety. *J. Agric. Food Chem.* **2009**, *57*, 1383–1388. [[CrossRef](#)] [[PubMed](#)]
22. Ouyang, G.; Chen, Z.; Cai, X.-J.; Song, B.-A.; Bhadury, P.S.; Yang, S.; Jin, L.-H.; Xue, W.; Hu, D.-Y.; Zeng, S. Synthesis and antiviral activity of novel pyrazole derivatives containing oxime esters group. *Bioorg. Med. Chem.* **2008**, *16*, 9699–9707. [[CrossRef](#)] [[PubMed](#)]
23. Wang, Y.; Zhang, J.; He, F.; Gan, X.; Song, B.; Hu, D. Design, synthesis, bioactivity and mechanism of dithioacetal derivatives containing dioxyether moiety. *Bioorg. Med. Chem. Lett.* **2019**, *29*, 2218–2223. [[CrossRef](#)] [[PubMed](#)]
24. Wang, Z.; Wei, P.; Liu, Y.; Wand, Q. D and E rings may not be indispensable for antofine: Discovery of phenanthrene and alkylamine chain containing antofine derivatives as novel antiviral agents against tobacco mosaic virus (TMV) based on interaction of antofine and TMV RNA. *J. Agric. Food Chem.* **2014**, *62*, 10393–10404. [[CrossRef](#)]
25. Wu, M.; Han, G.; Wang, Z.; Liu, Y.; Wang, Q. Synthesis and antiviral activities of antofine analogues with different C-6 substituent groups. *J. Agric. Food Chem.* **2013**, *61*, 1030–1035. [[CrossRef](#)]
26. Wang, Z.; Wei, P.; Xizhi, X.; Liu, Y.; Wang, L.; Wang, Q. Design, synthesis, and antiviral activity evaluation of phenanthrene-based antofine derivatives. *J. Agric. Food Chem.* **2012**, *60*, 8544–8551. [[CrossRef](#)]
27. Wang, Z.; Wang, L.; Ma, S.; Liu, Y.; Wang, L.; Wang, Q. Design, synthesis, antiviral activity, and SARs of 14-aminophenanthroindolizidines. *J. Agric. Food Chem.* **2012**, *60*, 5825–5831. [[CrossRef](#)]
28. Nagalakshamma, V.; Venkataswamy, M.; Pasala, C.; Umamaheswari, A.; Thyagaraju, K.; Nagaraju, C.; Chalapathi, P.V. Design, synthesis, anti-tobacco mosaic viral and molecule docking simulations of urea/thiourea derivatives of 2-(piperazine-1-yl)-pyrimidine and 1-(4-fluoro/4-chlorophenyl)-piperazine and 1-(4-chlorophenyl)-piperazine-A study. *Bioorg. Chem.* **2020**, *102*, 104084. [[CrossRef](#)]
29. Wang, D.; Huang, M.; Gao, D.; Chen, K.; Xu, W.; Li, X. Screening anti-TMV agents targeting tobacco mosaic virus Helicase Protein. *Pestic. Biochem. Physiol.* **2020**, *166*, 104449. [[CrossRef](#)]
30. Zhu, Y.-Y.; Yu, G.; Wang, Y.-Y.; Xu, J.-H.; Xu, F.-Z.; Fu, H.; Zhao, Y.-H.; Wu, J. Antiviral activity and molecular docking of active constituents from the root of *Aconitum Carmichaelii*. *Chem. Nat. Compd.* **2019**, *55*, 189–193. [[CrossRef](#)]
31. Wang, Z.; Wei, P.; Wang, L.; Wang, Q. Design, synthesis, and anti-tobacco mosaic virus (TMV) activity of phenanthroindolizidines and their analogues. *J. Agric. Food Chem.* **2012**, *60*, 10212–10219. [[CrossRef](#)] [[PubMed](#)]
32. Frisch, M.J.; Trucks, G.W.; Schlegel, H.B.; Scuseria, G.E.; Robb, M.A.; Cheeseman, J.R.; Scalmani, G.; Barone, V.; Petersson, G.A.; Nakatsuji, H.; et al. Gaussian 09, Revision, A.02, Inc., Wallingford CT, Wallingford. 2016. Available online: <https://gaussian.com/g09citation/> (accessed on 24 November 2021).
33. Molecular Operating Environment (MOE). 2015. Available online: <http://www.chemcomp.com> (accessed on 20 November 2021).
34. Becke, A.D. Density-functional thermochemistry. V. Systematic optimization of exchange-correlation functionals. *J. Chem. Phys.* **1997**, *107*, 8554–8560. [[CrossRef](#)]
35. Yongqin, X.; Schiele, B.; Akata, Z. Zero-shot learning the good, the bad and the ugly. In Proceedings of the IEEE Conference on Computer Vision and Pattern Recognition (CVPR), Salt Lake City, UT, USA, 21–26 July 2017; pp. 4582–4591.
36. Asurmendi, S.; Berg, R.H.; Koo, J.C. Coat protein regulates formation of replication complexes during tobacco mosaic virus infection. *Proc. Natl. Acad. Sci. USA* **2004**, *101*, 1415–1420. [[CrossRef](#)] [[PubMed](#)]
37. Reichel, C.; Beachy, R.N. Tobacco mosaic virus infection induces severe morphological changes of the endoplasmic reticulum. *Proc. Natl. Acad. Sci. USA* **1998**, *95*, 11169–11174. [[CrossRef](#)]
38. Sachse, C.; Chen, J.Z.; Coureux, P.D.; Stroupe, M.E.; Fändrich, M.; Grigorieff, N. High-resolution electron microscopy of Helical specimens: A fresh look at tobacco mosaic virus. *J. Mol. Biol.* **2007**, *371*, 812–835. [[CrossRef](#)]

39. Berman, H.M.; Westbrook, J.; Feng, Z.; Gilliland, G.; Bhat, T.N.; Weissig, H.; Shindyalov, I.N.; Bourne, P.E. The protein data bank. *Nucleic Acids Res.* **2000**, *28*, 235–242. [[CrossRef](#)]
40. Wang, J.; Wolf, R.M.; Caldwell, J.W.; Kollman, P.A.; Case, D.A. Development and testing of a general amber force field. *J. Comput. Chem.* **2004**, *25*, 1157–1174. [[CrossRef](#)]
41. Domingo, L.R.; Ríos-Gutiérrez, M.; Pérez, P. Applications of the conceptual density functional Theory indices to organic chemistry reactivity. *Molecules* **2016**, *21*, 748. [[CrossRef](#)]
42. Ramalho, T.C.; Caetano, M.S.; da Cunha, E.F.F.; Souza, T.C.S.; Rocha, M.V.J. Construction and assessment of reaction models of class I EPSP synthase: Molecular docking and density functional theoretical calculations. *J. Biomol. Struct. Dyn.* **2009**, *27*, 195–207. [[CrossRef](#)]
43. Kellenberger, E.; Rodrigo, J.; Muller, P.; Rognan, D. Comparative evaluation of eight docking tools for docking and virtual screening accuracy. *Proteins* **2004**, *57*, 225–242. [[CrossRef](#)]
44. Sturgeon, J.B.; Laird, B.B. Symplectic algorithm for constant-pressure molecular dynamics using a Nosé–Poincaré thermostat. *J. Chem. Phys.* **2000**, *112*, 3474–3482. [[CrossRef](#)]
45. Srivastava, R. Chemical reactivity theory (CRT) study of small drug-like biologically active molecules. *J. Biomol. Struct. Dyn.* **2021**, *39*, 943–952. [[CrossRef](#)] [[PubMed](#)]
46. Smith, R.D.; Engdahl, A.L.; Dunbar, J.B., Jr.; Carlson, H.A. Biophysical limits of protein–ligand binding. *J. Chem. Inf. Model.* **2012**, *52*, 2098–2106. [[CrossRef](#)] [[PubMed](#)]